New Phytologist

***New Phytologist* Supporting Information**

Article title: Plant nutrient-acquisition strategies drive topsoil microbiome structure and function
Authors: Mohammad Bahram, Tarquin Netherway, Falk Hildebrand, Karin Pritsch, Rein Drenkhan, Kaire Loit, Sten Anslan, Peer Bork, Leho Tedersoo
Article acceptance date: 31 March 2020

The following Supporting Information is available for this article:

Fig. S1. Distribution map of sampling plots.

Fig. S2. Principal coordinate analysis (PCoA) plot showing the variation in the composition of plant communities among samples (symbols).

Fig. S3. Pairwise Spearman correlations between environmental variables used in statistical analyses.

Fig. S4. Fungal communities drive bacterial and saprotrophic fungal communities and the abundance of pathogens.

Fig. S5. The main biotic and abiotic determinants of the relative abundance of nitrogen fixing and denitrifying bacteria.

Fig. S6. Functional guild composition of soil eukaryotes across plots dominated by different nutrient acquisition strategies.

Fig. S7. Random Forest heatmap indicates relationship of microbial taxa and functional groups to plant traits, edaphic, geographic and spatial variables.

Fig. S8. Functional and taxonomic composition of microbes differ between plant nutrient-acquisition strategies.

Fig. S9. Venn diagram based on the variation partitioning analysis of microbial taxonomic and functional composition.

Fig. S10. Diversity of carbohydrate-active enzymes (CAZymes) increases with increasing relative abundance of ectomycorrhizal plants.

Table S1. Samples used in this study.

Table S2. Results of structural equation modeling (SEM) shown in Fig. 2b.

Fig. S1. Distribution map of sampling plots.

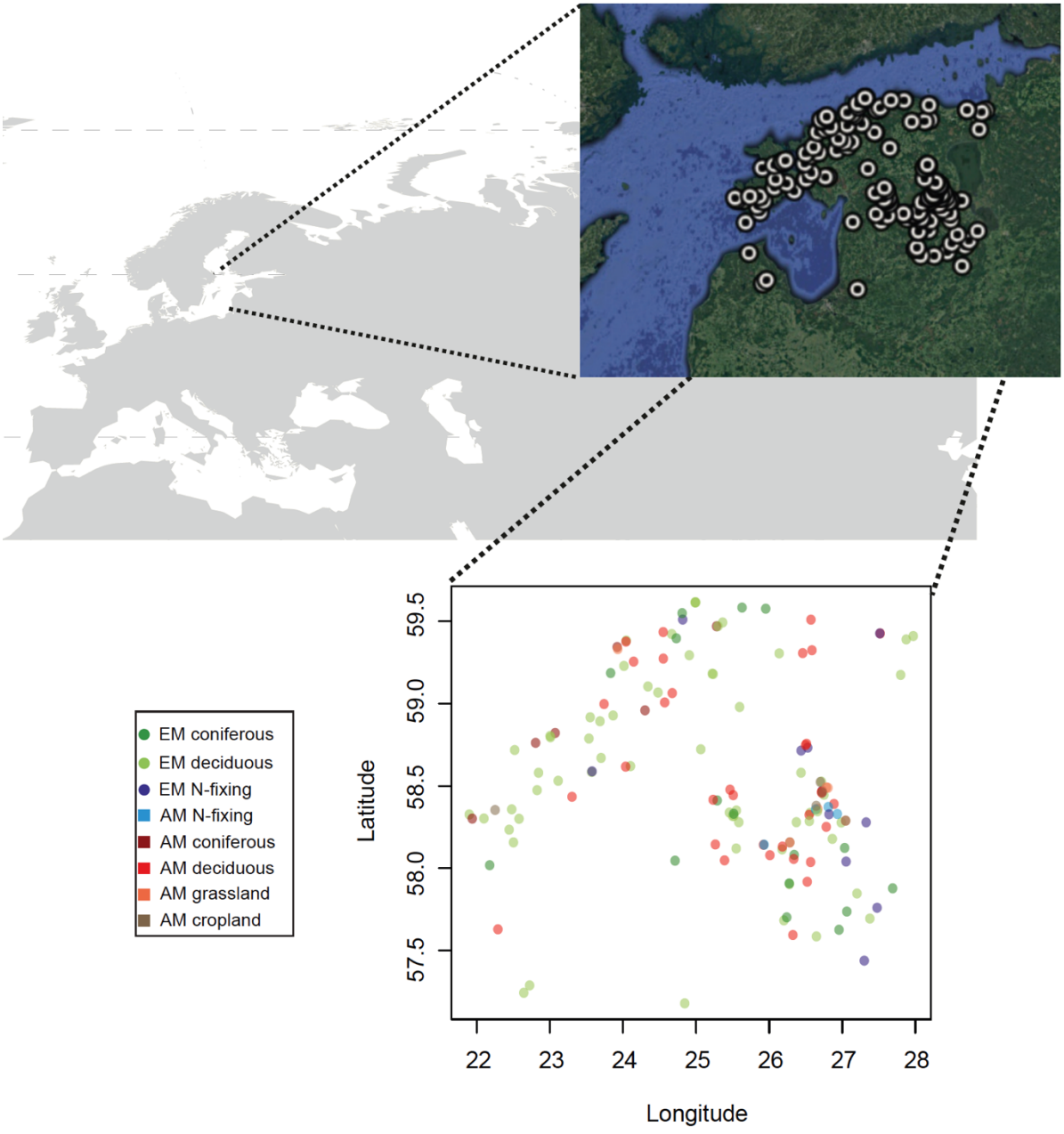

Fig. S2. Principal coordinate analysis (PCoA) plot showing the variation in the composition of plant communities among samples (symbols). Plant nutrient-acquisition strategies and the dominant vegetation type are shown in different colors as indicated in the legend.

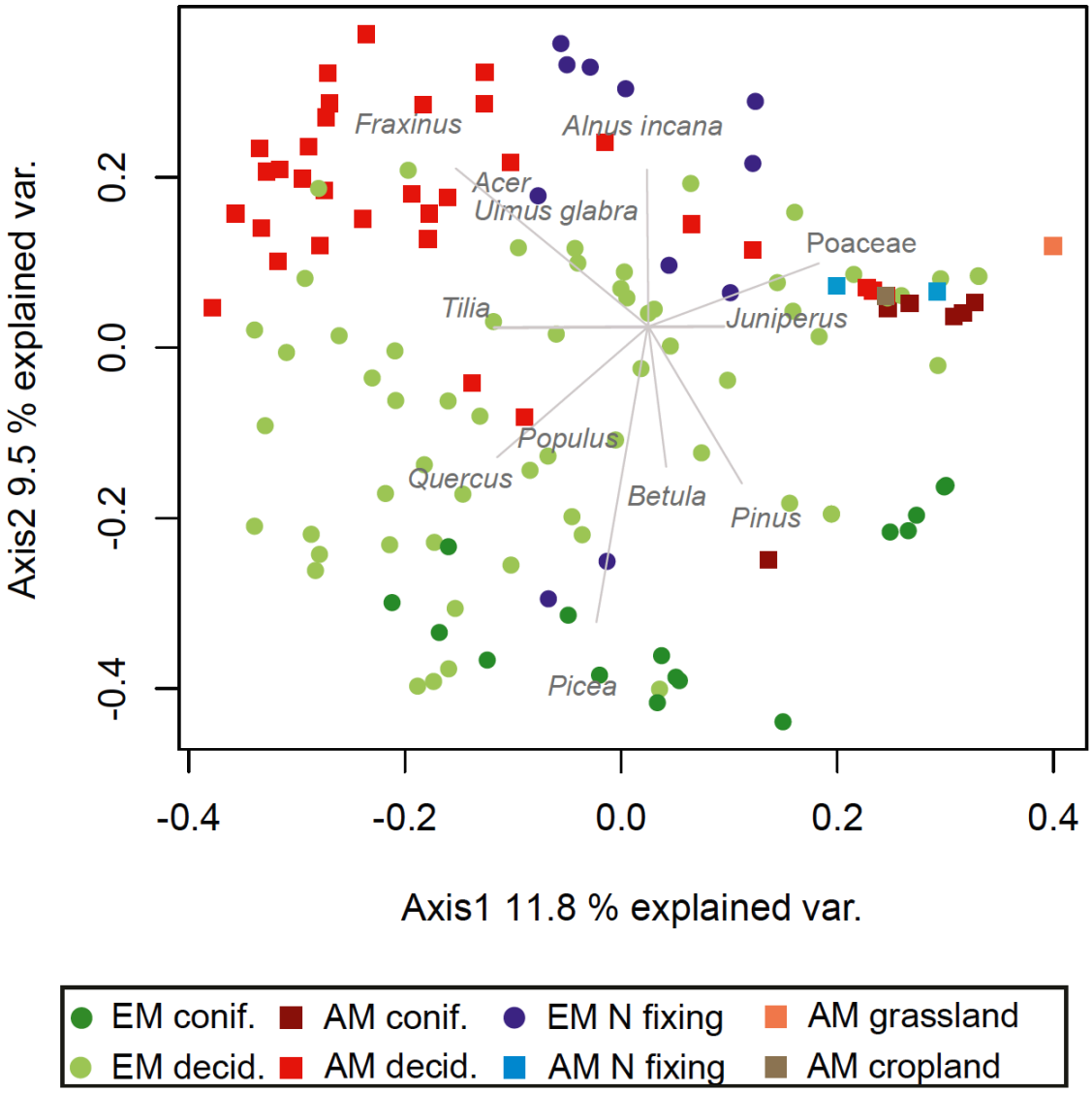

Fig. S3. Pairwise Spearman correlations between environmental variables used in statistical analyses. Non-significant correlations (adjusted p >0.1) are not shown. The different square sizes correspond to correlation coefficients (Spearman's rho).

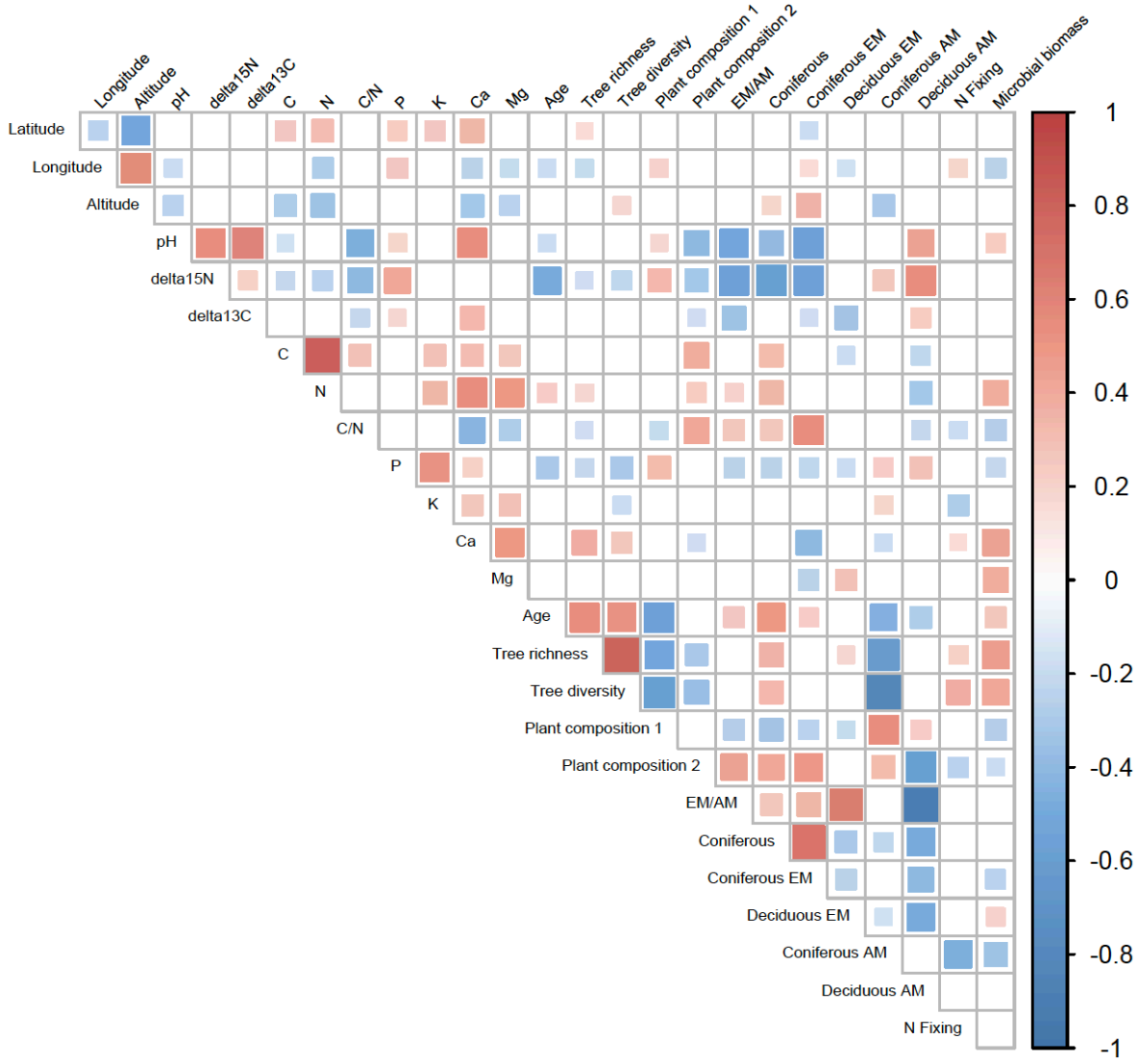

Fig. S4. Fungal communities drive bacterial and saprotrophic fungal communities and the abundance of pathogens. Best structural equation modeling (SEM) graphs indicating the direct and indirect relationships of richness (A) and community composition (B) of fungi and bacteria and the key determinant biotic and abiotic variables. All relationships were significant ($p<0.05$) and model fits were acceptable according to Chi-Square test ($p>0.1$) and PCLOSE test ($p>0.1$). For B, both directions between fungal and bacterial communities (represented by the first NMDS axis for each) were tested, and the model with fungal effect on bacterial community had lower AIC (40.24 vs 40.91, respectively). In addition, bacterial effect on fungal community was not significant when both directions were included in one model ($p=0.272$). In A, outlier C/N ratio values (>47), including two from grasslands (TR027,TR030) and four from croplands (TR036,TR047,TR051,TR065) were omitted.

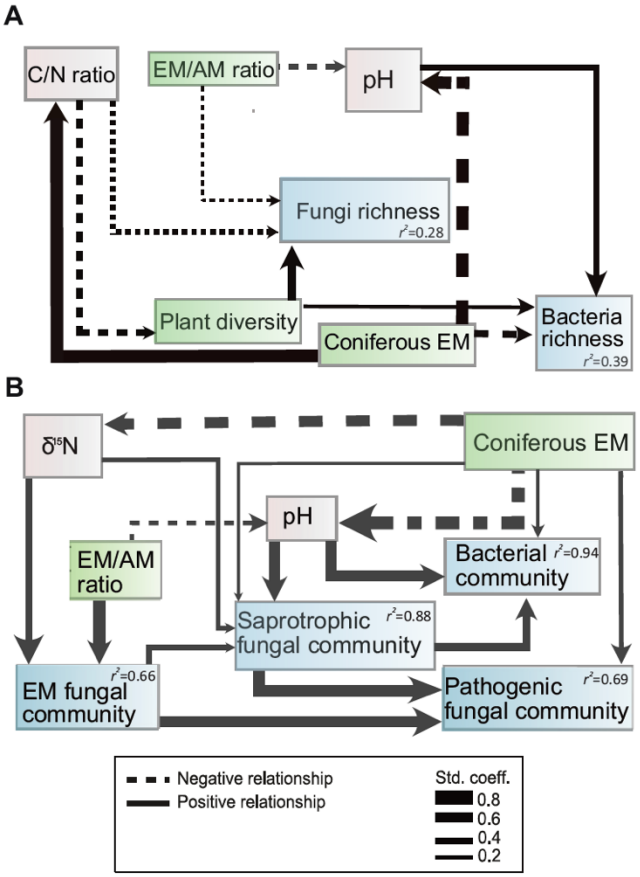

Fig. S5. The main biotic and abiotic determinants of the relative abundance of putative functional groups of bacteria. The size of circles corresponds to the variable importance based on Random Forest analysis (% of mean decrease accuracy estimated based on out-of-bag-CV). Blue and red colors show negative and positive Spearman correlations, with bubble diameter corresponding to relative correlation coefficient. The top barplot shows the out-of-bag variance explained for each model with the dependent variables on the x-axis.

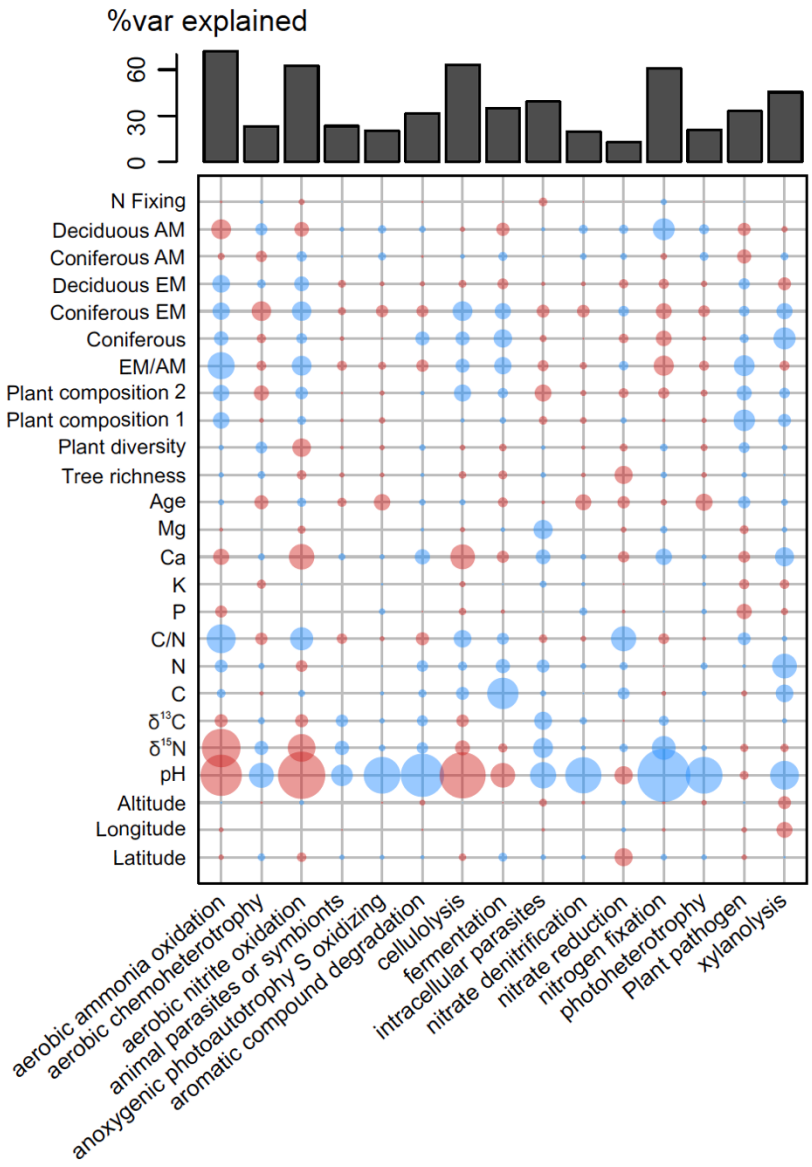

Fig. S6. Functional guild composition of soil eukaryotes across plots dominated by different nutrient acquisition strategies and the dominant vegetation type, by either including (A) or excluding (B) mycorrhizal fungi.

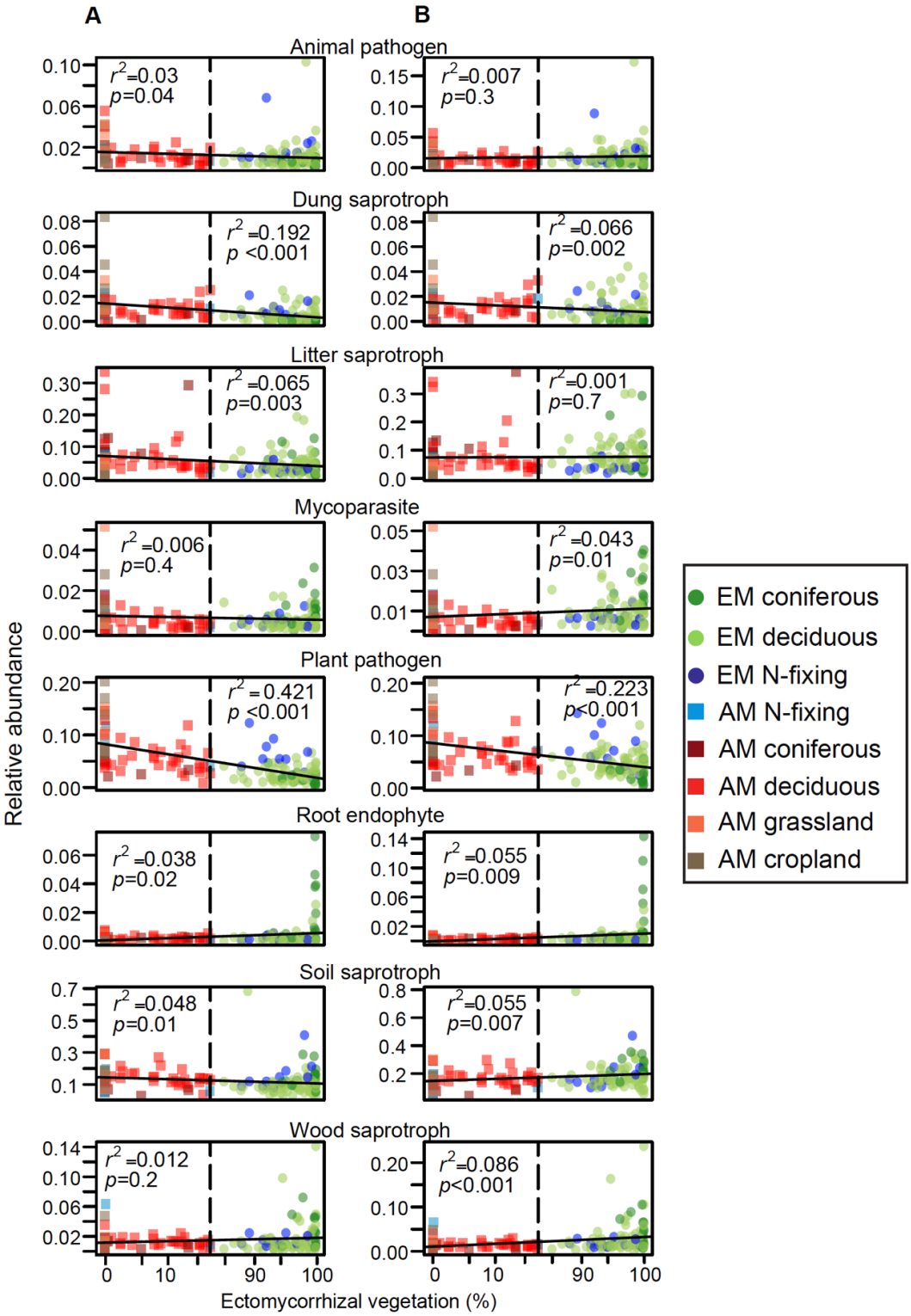

Fig. S7. Random Forest heatmap indicates relationship of microbial taxa and functional groups to plant traits, edaphic, geographic and spatial variables. Spatial variables are represented by PCNM vectors calculated based on geographic distance between samples (see Material and Methods in the main text). The size of circles corresponds to the variable importance (% of mean decrease accuracy estimated based on out-of-bag-CV); blue and red colours depict negative and positive Spearman correlations, respectively. Plant composition 1 & 2 are the first two PCA axes representing changes in the composition of plants across the plots.

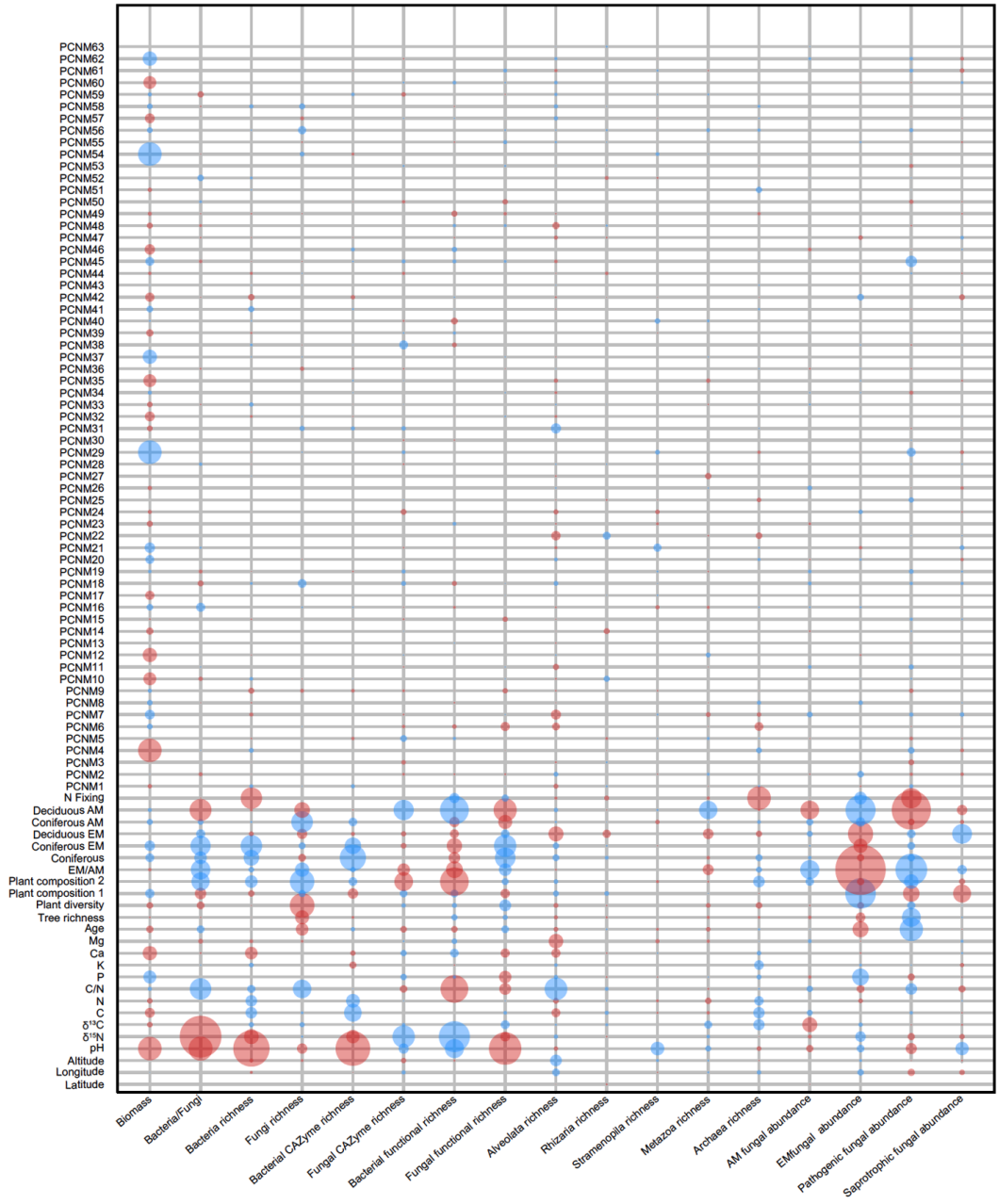

Fig. S8. Functional and taxonomic composition of microbes differ between plant nutrient-acquisition strategies and the dominant vegetation type. Bray-Curtis dissimilarities among samples (symbols) are illustrated based on non-metric multidimensional scaling (NMDS) of **A**) bacterial OTUs; **B**) fungal OTUs; **C**) Bacterial orthologous genes (OGs); **D**) fungal OGs; **E**) bacterial carbohydrate-active enzymes (CAZymes); **F**) fungal CAZymes. Colors and symbols represent plant functional types as indicated in the legend. Significant biotic and abiotic variables correlated to ordination axis (at $p<0.001$) are shown. Ellipses denote 95% confidence limits based on standard error of centroids in each category.

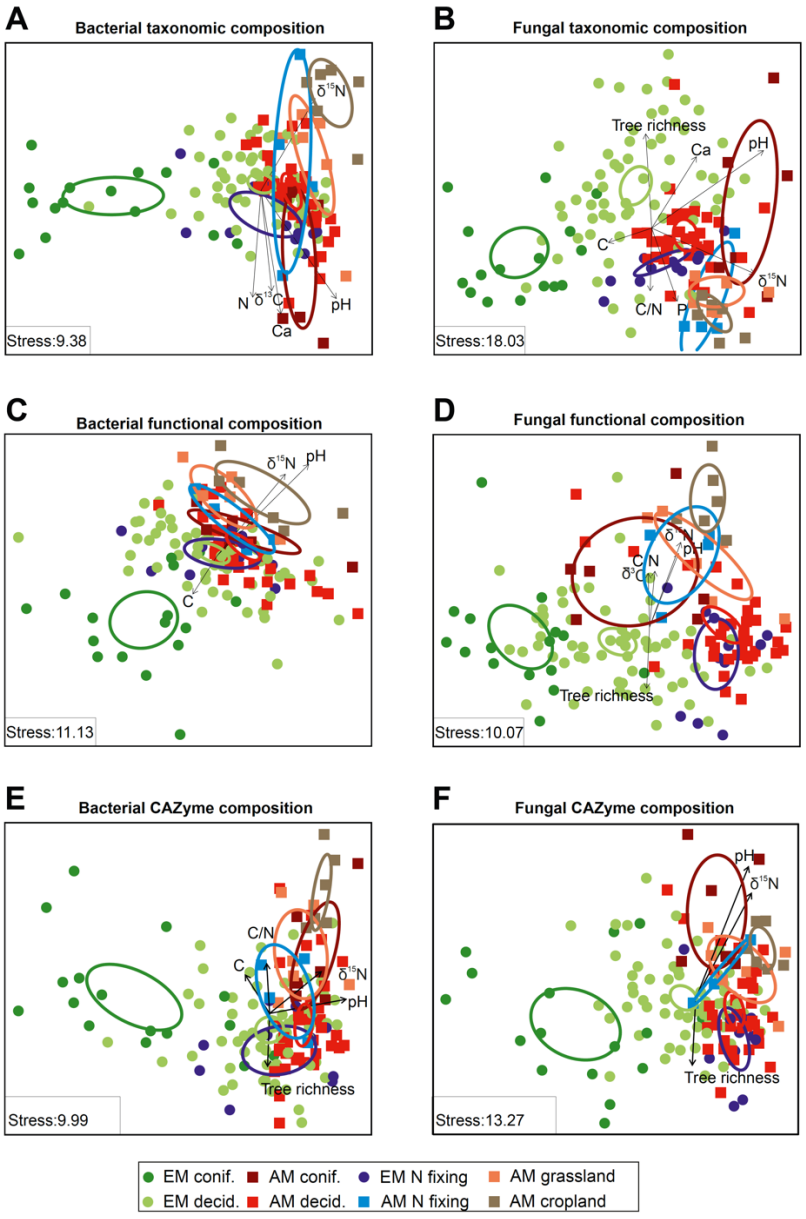

Fig. S9. Venn diagram based on the variation partitioning analysis of bacterial and fungal taxonomic (A,B, respectively) and functional (C,D, respectively) composition, showing the fraction of variation explained by soil, vegetation and spatial (PCNM) variables. Mantel test also revealed weak spatial autocorrelation in the composition of bacterial OTUs (r=0.085, p=0.022), fungal OTUs (r=0.159, p=0.001), bacterial OGs (r=0.073, p=0.035) and fungal OGs (r=0.042, p=0.056).

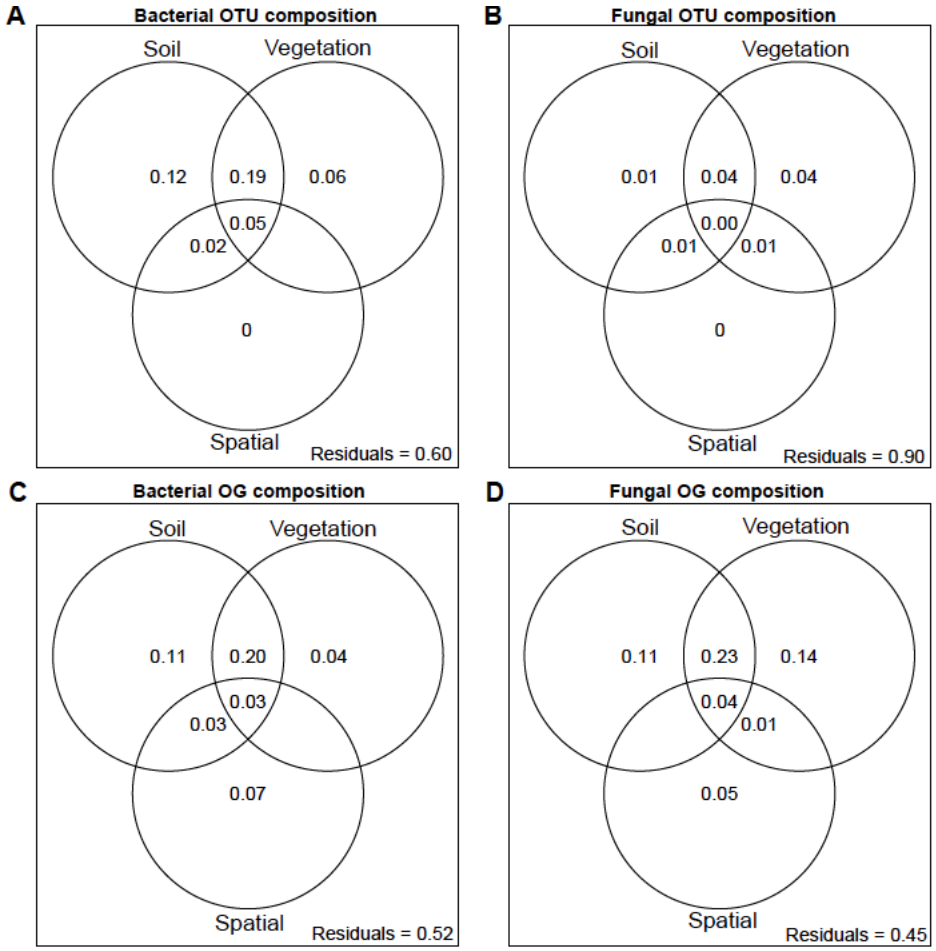

Fig. S10. Diversity of carbohydrate-active enzymes (CAZymes) increases with increasing relative abundance of ectomycorrhizal plants. Diversity is calculated based on Shannon index (after accounting for library size variation) for bacteria (A) and fungi (B).

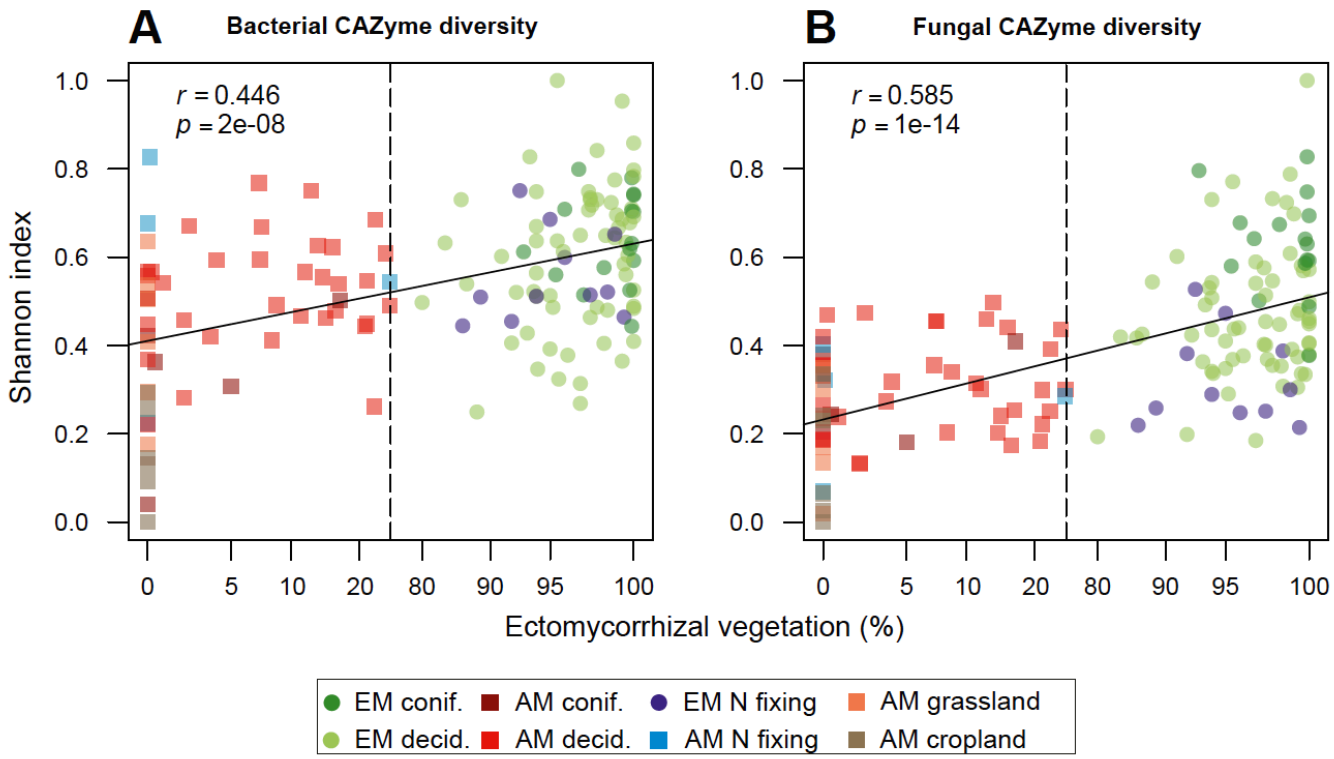

Table S1. Samples used in this study. The table presents a list of sample names and associated soil and vegetation parameters and other metadata. Plant community sheet show the relative abundance of plants in each plot. Plant community 1 and 2 are the first two axes from a principal coordinates analysis (PCoA) of plant community.
See separate Excel file.

Table S2. Results of structural equation modeling (SEM) shown in Fig. 2b. Model fitness was acceptable (ChiSquare =14.68, df=12, p=0.263; RMSEA=0.039, PCLOSE=0.558).

			Estimate	Standard. estimate	Composite Reliability	P
EM fungi	<---	EM/AM	.437	.034	12.929	<0.01
pH	<---	Coniferous EM	-3.155	.294	-10.725	<0.01
pH	<---	EM/AM	-1.472	.283	-5.199	<0.01
pH	<---	EM fungi	1.619	.459	3.526	<0.01
Bacteria/Fungi	<---	pH	.001	.000	4.474	<0.01
Bacteria/Fungi	<---	Coniferous EM	-.004	.001	-4.874	<0.01
Bacteria/Fungi	<---	EM fungi	-.003	.001	-4.757	<0.01
δ^{15}N	<---	Coniferous EM	-5.883	.937	-6.280	<0.01
δ^{15}N	<---	EM/AM	-2.134	.557	-3.832	<0.01
Saprotrophic fungi	<---	EM fungi	-.262	.029	-8.962	<0.01
δ^{15}N	<---	Bacteria/Fungi	196.605	100.190	1.962	.050
Pathogenic fungi	<---	pH	.008	.002	3.975	<0.01
Pathogenic fungi	<---	EM fungi	-.137	.013	-10.685	<0.01
Pathogenic fungi	<---	Saprotrophic fungi	-.087	.035	-2.480	.013
Saprotrophic fungi	<---	δ^{15}N	-.011	.003	-4.414	<0.01
δ^{15}N	<---	Saprotrophic fungi	6.045	2.892	2.090	.037